Microscopic investigation of the slurry drying process and binder migration in Li-ion battery anodes using multiscale-simulation methods

Sowmya Indrakumar[1], Jonas Breitenbach[2], Simone Rudolf[2], Jan-Willem Handgraaf[1], Larisa von Riewel[2]

1: Siemens Industry Software Netherlands B.V., Pr. Beatrixlaan 800, 2595 BN Den Haag, Netherlands
2: Heraeus Noblelight GmbH, Heraeusstraße 12, 63450 Hanau, Germany

Abstract:

The slurry drying process plays a crucial role in the manufacturing of lithium-ion battery electrodes, impacting properties such as porosity, electrode film characteristics, and performance. Substituting environmentally harmful and costly organic solvents such as N-methyl-2-pyrrolidone (NMP) with water, coupled with ongoing endeavors to reduce energy consumption and costs, has resulted in a surge of development activities in this domain. The integration of infrared emitters in the process of electrode drying presents a favorable strategy for optimizing both the physical and economic facets of the drying process simultaneously. This study employs multiscale-simulation methods, including molecular dynamics (MD) and dissipative particle dynamics (DPD) simulations, to explore binder migration, active layer adhesion, and the role of binders at varying drying rates. Results indicate good agreement with experimental findings, emphasizing the potential of this computational model to enhance battery formulations and process parameters in a cost-effective and sustainable manner at an early stage in the discovery process.

Keywords: Slurry drying, Molecular dynamics simulations, Dissipative particle dynamics, Li-ion batteries, Binders, binder migration, SBR, CMC, infrared drying.

1. Introduction

Lithium-ion batteries (LiB) play a vital role as electrochemical energy storage systems. These batteries are prevalent within portable devices such as mobile phones, and laptops, and are increasingly used in vehicles due to their relatively high power and energy density. Nevertheless, cell manufacturing processes are extremely complex with many controllable parameters, especially the slurry drying process during the production of electrode films.[1] The drying process of lithium-ion battery electrodes plays a critical role in determining the performance and durability of the batteries. Several electrode properties such as porosity and electrical conductivity, which directly result in the cell performance properties, evolve during the drying process, which makes it a crucial step in a cell manufacturing chain.[1]

The LiB electrodes are manufactured by casting a slurry onto a metallic current collector, for instance, a copper substrate for the anode side in this study. The steps involved in electrode manufacturing consist of mixing, coating, drying, calendaring, post-drying, and cell assembly. Typically, the slurry contains an active material (graphite – anode / metal oxide – cathode), conductive carbon material (carbon black / carbon nanotubes), different binder types and a solvent. After mixing, the resulting slurry is coated onto the current collector and then dried to create a porous electrode that is needed to fabricate the battery. Generally, CMC and SBR are used as additives in aqueous anode slurries to improve stability, processability, and electrochemical cell performance.[2] CMC is the main binder, while SBR particles are added for adhesion. CMC also contributes to the cohesive strength of the electrode layer.[2]

On the one side, the anode slurry is dissolved in an aqueous solvent. On the other hand, an organic solvent such as N-methyl-2-pyrrolidone (NMP) is used on the cathode side. The organic solvents (NMP) are environmentally unfriendly, flammable, and are often a cause of safety concerns. Furthermore, they are associated with high costs with their use in LiB production, particularly for the upcoming high-volume mass production of electric vehicles. Thus, these days water-based battery slurries have been developed as a promising environmentally friendly alternative.

Another issue currently discussed in industrial cost and energy savings segment, is the optimization of the drying process. Electrode properties and process speed are significantly restricted by heat and mass transfer mechanisms in conventional convective drying. That leads to slow and cost-intensive processes as a huge amount of hot air combined with adequate exhausting is needed. The use of infrared radiation is a promising approach to increase the efficiency of the drying-process, which directly involves a significant reduction of energy consumption and production costs.

In this study, we conduct theoretical and experimental investigations of the drying process of lithium-ion

battery anodes and examine the behaviour of film solidification and binder migration. We focus on the influence of the drying rates in terms of energy density on the mechanical stability of the electrode layer, measured as the adhesion force between electrode and current collector. Our experimental results are based on tests and analytical studies performed as described in section 2.6. To gain a fundamental understanding of the governing processes, we employ Simcenter Culgi [3]–[8] multiscale-simulation methods, namely, dissipative particle dynamics (DPD)[9] and molecular dynamics (MD) simulations, to conduct a microscopic analysis of the slurry drying process. Specifically, we investigate binder migration, adhesion of active layer onto the substrate, and the role of binders for two drying rates (slow or fast). Additionally, computational results are compared to the previously published experimental results [1] and [9]. Jaiser et. al. provide mechanistic insights into the slurry drying process and the impact of drying on the electrochemical properties [10]. In general, we see good agreement between the simulation and experimental findings. The enrichment of binder at the surface is observed for the fast-drying rates, which in turn is independent of the two fundamental processes, namely capillary action, and diffusion.[10]

2. Methodology

2.1 Starting structures

Atomistic representations for each of the components of the slurry were generated using Simcenter Culgi (Figure 1). The binder polymers namely, styrene butadiene rubber (SBR) and carboxymethyl cellulose (CMC) were constructed to the desired length using the homopolymer builder plugin inside Simcenter Culgi. The length of SBR and CMC polymer used in these simulations are 3 and 540 monomeric long, respectively (Figure 2). The active materials used in the slurry are SiO_2 (Silicon dioxide) and an active carbon material. As conductive additives, graphite sheets and carbon nanotubes were added. They are represented as colloidal entities, coordinates of which are fixed in space and have restricted degrees of freedom (Figure 2).

2.2 Automated Fragmentation and Parameterisation

The atomic structures of slurry components were taken further for automated fragmentation [3] and parameterisation (AFP) using the new potential energy function describing both the attractive and repulsive intermolecular forces. The classical soft repulsive intermolecular Van-der-Waals DPD potential allows for high time and space scale modeling but cannot capture phase transitions as it is essentially emulating a super-condensed gas. Moreover, the oversimplified form of the potential doesn't allow for multi-variant parameterization since the intermolecular a-parameters are effectively determining the system's behavior to its entirety. To overcome these limitations, we propose a new intermolecular Van-der-Waals interaction that includes an attractive well inspired by the Lennard-Jones potential. This approach allows for modeling of all phases at physiologically representative temperature and pressure values. We used a three-to-one mapping of heavy atoms to coarse-grained beads.

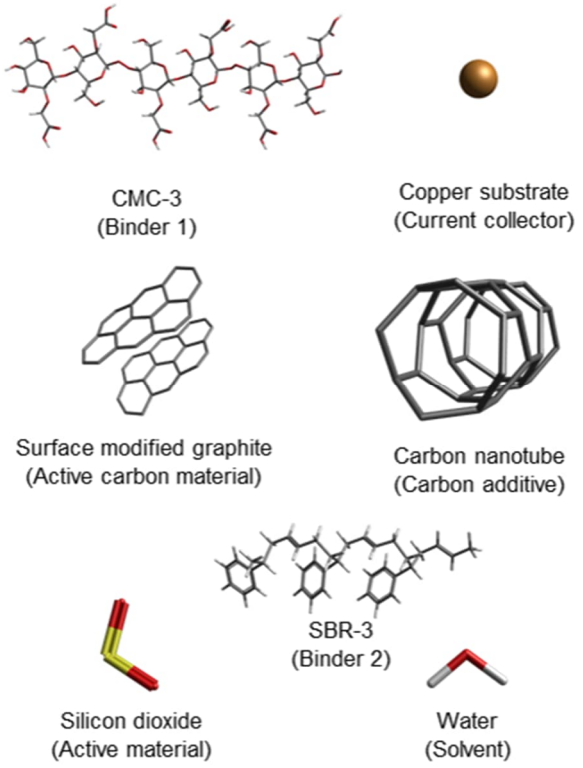

Figure 1: Atomic structures of slurry components used to derive coarse grained inter and intra molecular interactions.

2.3 Computational IR spectra

IR spectra of the atomic structures were calculated using the NWChem plugin inside Simcenter Culgi. Initially, the structures were geometry optimised with the Hartree Fock (HF) ab-initio method using 6-31G* atomic orbitals basis set. Subsequently, the IR spectra were calculated alongside energy optimisation using the same basis set.

2.4 Dissipative Particle Dynamics (DPD)

The DPD simulations were performed using the Simcenter Culgi software.[4] The DPD time step was set to 0.01, pressure was set to 0.011 (1 atm), and the Andersen piston friction and Andersen friction mass was set to 0.05 and 0.002, respectively. Intermolecular and intramolecular parameters were obtained through the AFP protocol outlined in section 2.2. The box size was set to Lx = Ly = 60 and

L_Z=69 (DPD units; cell size, rc = 7.66 Å). First, the system was equilibrated using canonical (NVT) ensemble for 10^5 steps followed by NPT for $3*10^5$ steps. Following this, the system was dried using two methods: slow and fast heating. In the slow heating approach, the system was incrementally heated from 1 to 1.9 (DPD units; 1DPD = 298K) with an increment of 0.3 DPD unit at each step. Conversely, during fast heating, the system was heated directly from 25°C to 270°C in one step. The slurry composition employed in these simulations mirrored that of the experimental setup. Each heating step was run for $9*10^5$ steps. After heating, the production step was run for $5*10^5$ steps. The analyses were performed on the dried slurry from the production run using Simcenter Culgi. The binder diffusion coefficient on the dried slurry was calculated using the methodology described previously.[4]

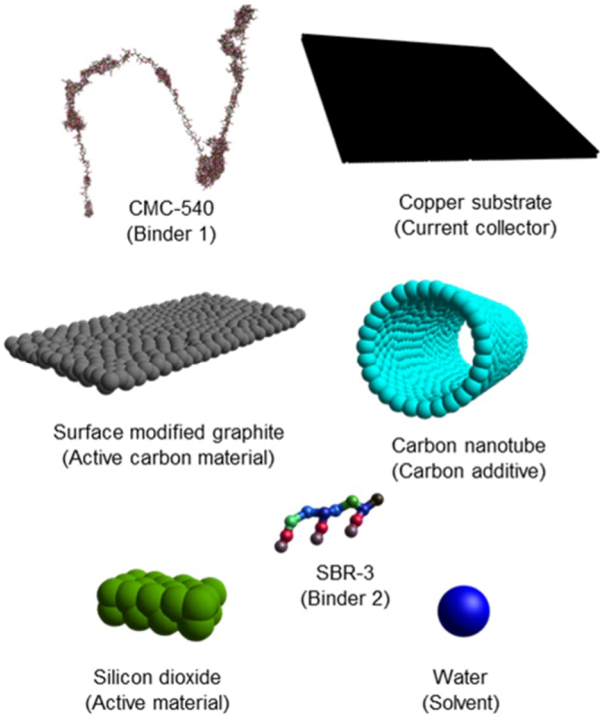

Figure 2: Coarse-grained structure of slurry components used for DPD slurry drying simulations.

2.5 Molecular Dynamics Simulations

To validate the developed coarse-grained model, a set of classical all-atom Molecular Dynamics (MD) simulations were conducted in explicit solvent to generate an ensemble of dried slurry formulation. The water content of the slurry was set to 2% mass fraction, which corresponded to the amount of water left behind after slurry had dried in both DPD simulations and experimental observations. The dreiding [11] forcefield was utilized to model the slurry drying process. The MD simulations were performed on a copper crystal surface obtained from XDatabase [12] with reference no. 0011145, and the mass fractions of the slurry components (excluding water) were identical to the experimental mass fractions. Prior to simulation, the system was energy minimized using the MEMcalculator within Simcenter Culgi. The smooth particle mesh Ewald method[13] was employed to determine the non-bonded electrostatics energies, with a real-space cutoff of 7.5 Å. The system was then equilibrated at a constant volume for 50 ps at 300K, with a timestep of 0.5 fs, using the Andersen thermostat and barostat, with coordinates saved every 1000 steps. Subsequently, the system was equilibrated for another 150 ps at a constant pressure of 1atm and temperature of 300K. Finally, production simulations were carried out at the two drying rates for 150 ps, with coordinates saved every 1000 steps.

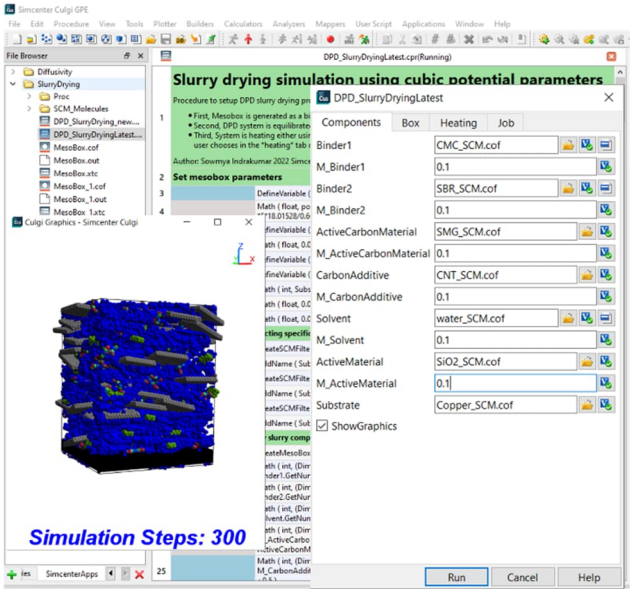

Figure 3: Simcenter Culgi application to run slurry drying simulations. User needs coarse-grained structures and parameter file as input to run the simulation. An example representation of the mass fractions of the slurry components is shown in this figure.

2.6 Slurry producing and drying experimental setup

To obtain a sufficiently high grade of dispersion of the ingredients (42,4% active material, 2,1% binder and 55% solvent) during the production of the electrode slurry, the paste was produced with the help of a speed mixer (DAC 1100, Hauschild). The applied stirring speed was up to 1500 min^{-1} with a mixing time of about 5 minutes. The homogenised electrode slurry was applied to a current collector using an automatic laboratory coater (MSK-AFA-II-VC, MTI-Corporation). This ensured an error-free electrode layer as well as a constant layer thickness, necessary for the further series of tests. The thickness of the wet electrode layer was approximately 160 µm. Directly following coating, the layer was dried in a dynamic drying process using infrared radiation (IR). We used an

infrared module consisting of six short-wave twin-tube emitters (Heraeus Noblelight GmbH) that had been installed parallel to the drying direction and delivered a total area output of 100 kW/m². For targeted and flawless drying, different drying intensities (realised by varying power densities 11 / 22 / 33 / 66 kW/m² and dedicated web speeds) were tested and compared with the simulation results. The drying rate of the slurry is directly correlated to the Energy density of the Heat flux.[14] After drying, the anode layers were calendered to a target density of approximately 1.5 to 1.6 g/cm³ (GK300L, SAUERESSIG Group). The fully calendered electrode was then subjected to a peel test to confirm the quality and performance of the dried electrode. The adhesion test performed was used to assess the adhesion force of the coated electrode to the current collector. This purely mechanical parameter was obtained using a 90° peel test method. All adhesion tests were carried out using a universal testing machine LS1 (AMETEK Inc).

3. Results and Discussions

3.1 Comparison of Infrared spectra (IR)

The IR spectra obtained using the NWChem plugin was compared to the experimental IR spectra of the aqueous slurry. Spectral analysis (attenuated total reflectance Fourier transformation infrared (ATR-FTIR)) of the slurry within a wavenumber range of 4500 to 160 cm^{-1} was used to identify the chemical functional groups present in the water-based slurry mixture. The measured transmittance spectrum (Figure 4a) shows a broad peak at 3200 cm^{-1} and a sharp peak at 1629 cm^{-1}. Those peaks can be referred to the stretching and bending vibrations of the O-H bonds in the water molecules.

In contrast to the experimental spectra, the NWChem IR spectra are calculated in vacuum and do not display peak broadening (Figure 4b). Furthermore, NWChem conducts IR spectra calculations for each molecule individually. This method enables clear visualization of distinct vibrations such as bond stretching and scissoring for different functional groups, allowing for precise identification, and labelling of different IR peaks. For example, the peak below 1000 cm^{-1} is attributed to the O-H bending of ether groups and in water molecules, peaks in the 1000-2000 cm^{-1} range are attributed to $-CH_2$ scissoring and COO- symmetric stretching, and peaks around 3200 cm^{-1} represent an average over O-H and C-H bond stretching peaks.

3.2 Peel Force

Figure 5 shows the adhesion force of the dried electrode layer to the current collector in dependence of the power density used for drying. The adhesion tests were carried out directly after drying and calendering. It is evident that when the power density of the emitter field increases, there is a reduction in the peel strength between the current collector and the electrode layer. Thus, a reduced adhesive strength can be observed with an increased electrical power density. Conversely, an increased adhesive strength of the electrode layer can be observed when using a low power output and thus slower drying speed.

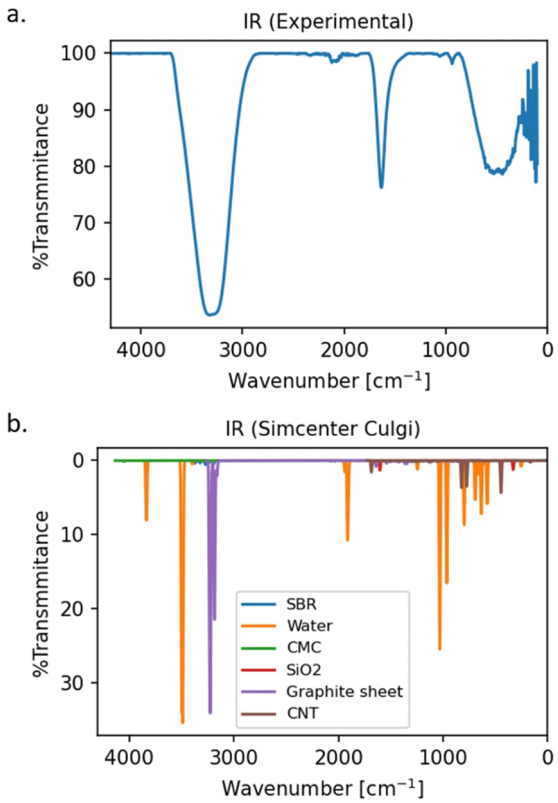

Figure 4: a) ATR-FTIR transmission spectrum of the aqueous slurry. b) The IR spectra of individual components obtained from the NWChem plugin.

3.3 Dissipative Particle Dynamics (DPD)

DPD simulations were performed to investigate the microscopic properties of the slurry drying process under two drying rates (Figure 6): slow heating, which represents heating with moderate energy densities, and fast heating, which represents high radiomagnetic energy input. In slow heating, system was heated from 1 to 1.9 DPD with an increment of 0.3 DPD step. In contrast, during fast heating, the system was directly heated from 1 to 1.9 DPD units in one step. The slurry composition employed in these simulations were similar to those of the experimental setup. Our findings indicated considerable differences in system behaviors depending on the drying rate. For instance, in the DPD simulations, we observed that the distribution of the SBR binder was more uniform during fast heating, whereas during slow heating, it tended to accumulate on the copper substrate (Figure 7a). This increased accumulation of SBR on the

copper substrate was caused by the lower diffusion of the binder under slow drying rates (Figure 7b), which consequently resulted in a stronger interaction between the SBR binder and copper (Figure 7c). SBR is the slurry component that is responsible for the adhesion of the electrode materials to the current collector. [2] In addition, Section 3.2 confirmed that the results obtained from the peel test were consistent with the findings from simulations, providing further evidence that the interaction between SBR and copper is affected by the drying conditions. Water was prone to phase separation from the rest of the slurry formulations and migrated towards the surface, resulting in its evaporation (Figure 6). As the slurry dried, water that phase separated and rose to the surface was removed, allowing the bulk water to phase separate (Figure 6). Regardless of the heating rate, some traces of water were left behind in the dried slurry (Figure 6c). Similarly, in experimental testing, we found that small amounts of water (2-3 %) remained trapped in the dried slurry. Additionally, during DPD simulations, we observed that slower heating rates resulted in a reduced moisture content compared to faster heating rates. The active carbon materials, SMG sheets, tended to stack together, whereas carbon additive (CNT) is homogenously distributed. Regardless of the heating process, traces of water remained post heating. Upon examining the CMC distribution during drying, we observed that it preferred to be at the interface of SMG sheets and water.

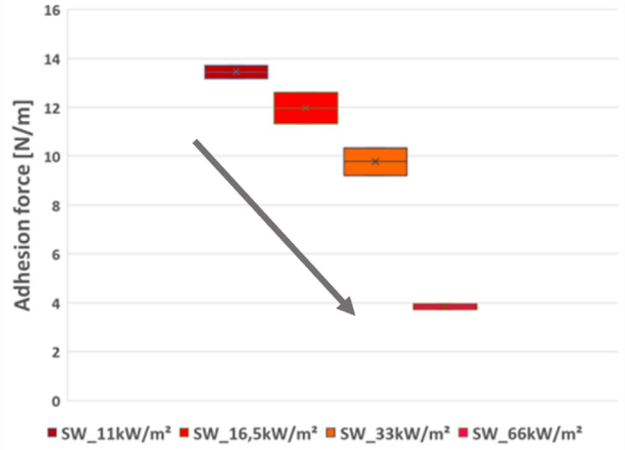

Figure 5: Box plot showing a decrease of the adhesion force with increasing power density for four different drying intensities.

Additionally, the CMC polymer was more compact in slow heating than in fast heating, with an average radius of gyration of 24 Å compared to 38 Å, respectively. The CMC molecules adhere to the active carbon material. This connection leads to sufficient electrical conductivity as well as cohesion in the dried electrode layer.[2] The nature of CMC compaction that is reflected in the radius of gyration directly influences the electrical and mechanical properties of the electrode.

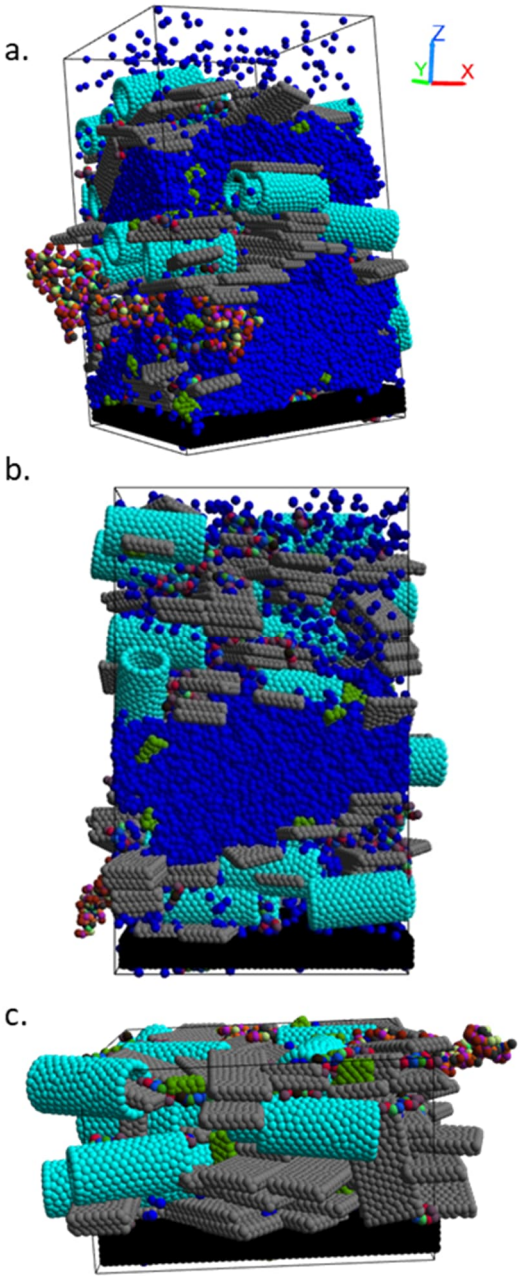

Figure 6: a) slurry drying snapshot taken from the start of the DPD simulations. b) snapshot taken during the slurry drying state. c) dried slurry snapshot of the coarse-grained system. The components of the slurry are assigned the following colors: blue for water, cyan for CNT, gray for SMG, green for DMSO, and multi-colored beads for SBR and CMC.

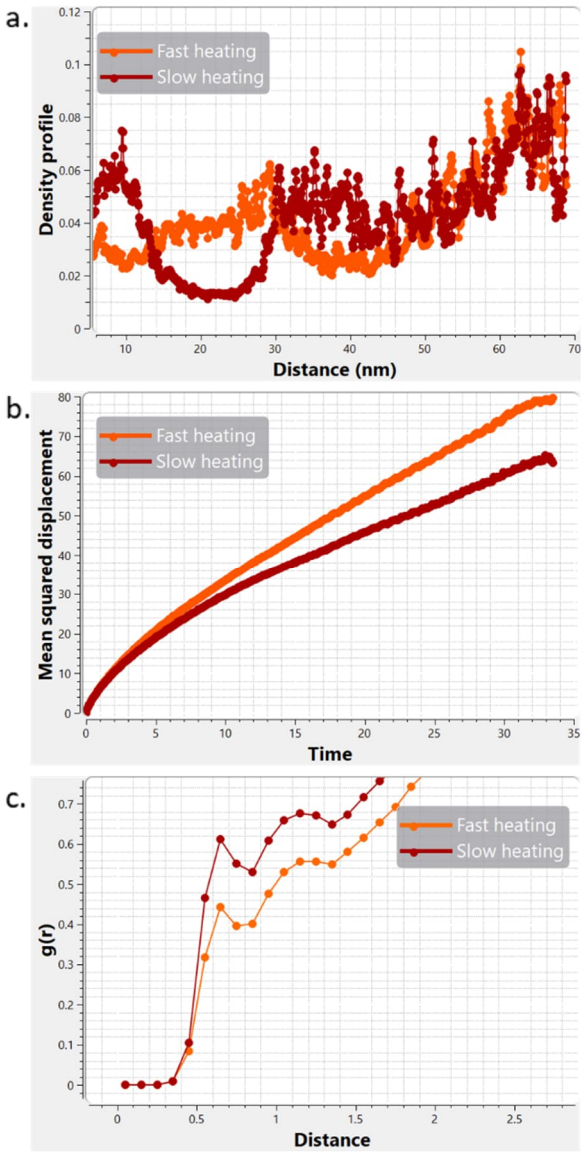

Figure 7: a) Density profile of SBR binder in the z-direction at different heating rates. B) mean squared displacement of SBR binder under different heating conditions. c) paired correlation function between SBR binder and copper substrate for the different heating rates.

3.4 Molecular dynamics (MD)

Molecular dynamics simulations were conducted on the dried slurry using two drying rates that were similar to those used in DPD simulations. The size of the slurry components was reduced significantly in comparison to the DPD simulations due to computational constraints. The main objective of these simulations was to verify the migration of the SBR binder at the molecular level. Figure 8a depicts the MD setup snapshot of the dried slurry, and it was observed that fast heating resulted in faster SBR migration compared to slow heating (Figure 8b). The absence of significant changes in the binder distribution on the copper substrate can be attributed to shorter sampling and the size of the system and slurry components (Figure 8c). This highlights the limitations of MD simulations, which require longer length and time scales to observe significant changes in the slurry morphology as observed in DPD simulations.

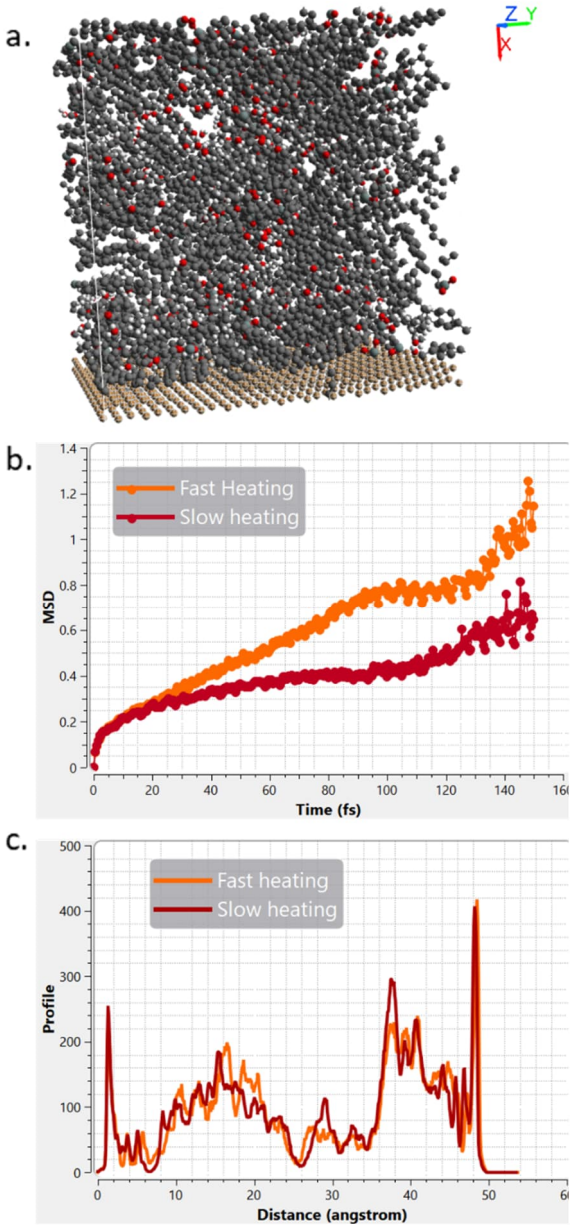

Figure 8: a) MD snapshot of the dried slurry system. B) mean squared displacement of SBR binder under different heating conditions. c) SBR binder density profile in the x-direction at different heating rates.

4. Conclusion

A new multiscale computational model was deployed to investigate microscopic properties of anode slurry drying using Simcenter Culgi. The findings reveal differences in binder migration under two different

drying rates, namely slow and fast heating rates. Slow heating leads to accumulation of the SBR binders on the copper substrate, whereas fast heating rates causes a decrease of SBR density at the slurry electrode interface and implicitly a loss of adhesion of SBR. Dense SBR accumulation on the copper substrate is driven from stronger favourable interactions of SBR with the copper substrate in slow heating as opposed to fast drying rate. Strong interactions between SBR and copper lead to high adhesion forces of the binder material to the substrate. This finding matches very well the experimentally determined dependence of the peeling force on the drying conditions. CMC binder prefers to be at the interface of SMG and water, which phase separates and rises to the surface, leading to its evaporation. This developed protocol is very generic and is applicable to any coating and drying of particulate dispersions for applications in e.g., paper coating, latex films, or LiB electrodes manufacturing industries.

In conclusion, the proposed computational model can be applied to better understand battery manufacturing processes early in the discovery stage to optimize formulations considering their full complexity. This approach can be readily incorporated to safely design sustainable batteries cost-effectively alongside saving on extensive experimentation. The results of our study provide insights into how to optimize the drying process to improve the performance and durability of lithium-ion batteries.

5. Acknowledgement

The authors would like to thank Siemens Industry Software Netherlands, B.V. for the computer resources used to perform the simulations. The authors would like to give special thanks to Dr. Jan van Male, Panos Petris, and Dr. Paul Becherer for their useful feedback and a nice discussion. Furthermore, the authors would like to thank the Heraeus Noblelight GmbH for the financial support of this project. Concerning the experimental parts of this study, special thanks go to Dr. Moritz Hantel und Dr. Benjamin Kruener of Heraeus Battery Technology for their help and support.

6. References

[1] Y. S. Zhang *et al.*, “A Review of Lithium-Ion Battery Electrode Drying: Mechanisms and Metrology,” *Adv. Energy Mater.*, vol. 12, no. 2, p. 2102233, Jan. 2022, doi: 10.1002/aenm.202102233.

[2] R. Gordon, R. Orias, and N. Willenbacher, “Effect of carboxymethyl cellulose on the flow behavior of lithium-ion battery anode slurries and the electrical as well as mechanical properties of corresponding dry layers,” *J. Mater. Sci.*, vol. 55, no. 33, pp. 15867–15881, Nov. 2020, doi: 10.1007/s10853-020-05122-3.

[3] J. G. E. M. Fraaije, J. van Male, P. Becherer, and R. Serral Gracià, “Coarse-Grained Models for Automated Fragmentation and Parametrization of Molecular Databases,” *J. Chem. Inf. Model.*, vol. 56, no. 12, pp. 2361–2377, Dec. 2016, doi: 10.1021/acs.jcim.6b00003.

[4] J. G. E. M. Fraaije, J. van Male, P. Becherer, and R. Serral Gracià, “Calculation of Diffusion Coefficients through Coarse-Grained Simulations Using the Automated-Fragmentation-Parametrization Method and the Recovery of Wilke–Chang Statistical Correlation,” *J. Chem. Theory Comput.*, vol. 14, no. 2, pp. 479–485, Feb. 2018, doi: 10.1021/acs.jctc.7b01093.

[5] P. C. Petris, P. Becherer, and J. G. E. M. Fraaije, “Alkane/Water Partition Coefficient Calculation Based on the Modified AM1 Method and Internal Hydrogen Bonding Sampling Using COSMO-RS,” *J. Chem. Inf. Model.*, vol. 61, no. 7, pp. 3453–3462, Jul. 2021, doi: 10.1021/acs.jcim.0c01478.

[6] A. J. M. Sweere, B. Patham, V. Sugur, and J. Handgraaf, “A Multiscale Approach for Estimating Permeability Properties of Polymers with Complex Aromatic Backbones: A Case Study on Diffusivity of Small Gas Molecules in Polyphenylene Ether,” *Macromol. Theory Simulations*, p. 2000027, Jun. 2020, doi: 10.1002/mats.202000027.

[7] V. Y. Hon *et al.*, “Microemulsion interface model for chemical enhanced oil recovery design,” *J. Pet. Sci. Eng.*, vol. 212, p. 110279, May 2022, doi: 10.1016/j.petrol.2022.110279.

[8] G. Scocchi, P. Posocco, J.-W. Handgraaf, J. G. E. M. Fraaije, M. Fermeglia, and S. Pricl, “A Complete Multiscale Modelling Approach for Polymer-Clay Nanocomposites,” *Chem. - A Eur. J.*, vol. 15, no. 31, pp. 7586–7592, Aug. 2009, doi: 10.1002/chem.200900995.

[9] R. D. Groot and P. B. Warren, “Dissipative

particle dynamics: Bridging the gap between atomistic and mesoscopic simulation," *J. Chem. Phys.*, vol. 107, no. 11, pp. 4423–4435, Sep. 1997, doi: 10.1063/1.474784.

[10] S. Jaiser, M. Müller, M. Baunach, W. Bauer, P. Scharfer, and W. Schabel, "Investigation of film solidification and binder migration during drying of Li-Ion battery anodes," *J. Power Sources*, vol. 318, pp. 210–219, Jun. 2016, doi: 10.1016/j.jpowsour.2016.04.018.

[11] S. L. Mayo, B. D. Olafson, and W. A. Goddard, "DREIDING: a generic force field for molecular simulations," *J. Phys. Chem.*, vol. 94, no. 26, pp. 8897–8909, Dec. 1990, doi: 10.1021/j100389a010.

[12] M. Downs, Robert T.; Hall-Wallace, "The American Mineralogist crystal structure database," *Am. Mineral.*, vol. 88, pp. 247–250, 2003.

[13] U. Essmann, L. Perera, M. L. Berkowitz, T. Darden, H. Lee, and L. G. Pedersen, "A smooth particle mesh Ewald method," *J. Chem. Phys.*, vol. 103, no. 19, pp. 8577–8593, Nov. 1995, doi: 10.1063/1.470117.

[14] A. Altvater, T. Heckmann, J. C. Eser, S. Spiegel, P. Scharfer, and W. Schabel, "(Near-) Infrared Drying of Lithium-Ion Battery Electrodes: Influence of Energy Input on Process Speed and Electrode Adhesion," *Energy Technol.*, p. 2200785, Sep. 2022, doi: 10.1002/ente.202200785.

7. Glossary

DPD: Dissipative Particle Dynamics
MD: Molecular Dynamics
CMC: carboxymethyl cellulose
SBR: styrene butadiene rubber
NMP: N-methyl-2-pyrrolidone
CNT: Carbon Nanotube
LiB: Lithium-ion battery
AFP: Automated Fragmentation and Parameterisation
IR: Infrared spectra
SMG: Surface Modified Graphite